


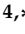



Article

# [Cr<sup>III</sup><sub>8</sub>Ni<sup>II</sup><sub>6</sub>]<sup>n+</sup> Heterometallic Coordination Cubes

Helen M. O'Connor <sup>1</sup>, Sergio Sanz <sup>1</sup>, Aaron J. Scott <sup>1</sup>, Mateusz B. Pitak <sup>2</sup>, Wim T. Klooster <sup>2</sup>, Simon J. Coles <sup>2</sup>, Nicholas F. Chilton <sup>3</sup>, Eric J. L. McInnes <sup>3</sup>, Paul J. Lusby <sup>1</sup>, Høgni Weihe <sup>4</sup>, Stergios Piligkos <sup>4,\*</sup>, and Euan K. Brechin <sup>1,\*</sup>

<sup>1</sup> EaStCHEM School of Chemistry, The University of Edinburgh, David Brewster Road, Edinburgh EH3 5JF, UK; oconnoh7@tcd.ie (H.M.O.); s.calvo@fz-juelich.de (S.S.); Aaron.Scott@ed.ac.uk (A.J.S.); Paul.Lusby@ed.ac.uk (P.J.L.)

<sup>2</sup> UK National Crystallography Service, Chemistry, Highfield Campus, University of Southampton, Southampton SO17 1BJ, UK; Mateusz.Pitak@matthey.com (M.B.P.); W.T.Klooster@soton.ac.uk (W.T.K.); S.J.Coles@soton.ac.uk (S.J.C.)

<sup>3</sup> Department of Chemistry, The University of Manchester, Oxford Road, Manchester M13 9PL, UK; nicholas.chilton@manchester.ac.uk (N.F.C.); eric.mcinnnes@manchester.ac.uk (E.J.L.M.)

<sup>4</sup> Department of Chemistry, University of Copenhagen, Universitetsparken 5, Copenhagen DK-2100, Denmark; weihe@chem.ku.dk

\* Correspondence: piligkos@kiku.dk (S.P.); ebrechin@ed.ac.uk (E.K.B.)

**Abstract:** Three new heterometallic [Cr<sup>III</sup><sub>8</sub>Ni<sup>II</sup><sub>6</sub>] coordination cubes of formulae [Cr<sup>III</sup><sub>8</sub>Ni<sup>II</sup><sub>6</sub>L<sub>24</sub>(H<sub>2</sub>O)<sub>12</sub>](NO<sub>3</sub>)<sub>12</sub> (**1**), [Cr<sup>III</sup><sub>8</sub>Ni<sup>II</sup><sub>6</sub>L<sub>24</sub>(MeCN)<sub>7</sub>(H<sub>2</sub>O)<sub>5</sub>](ClO<sub>4</sub>)<sub>12</sub> (**2**), and [Cr<sup>III</sup><sub>8</sub>Ni<sup>II</sup><sub>6</sub>L<sub>24</sub>Cl<sub>12</sub>] (**3**) (where HL = 1-(4-pyridyl)butane-1,3-dione), were synthesised using the paramagnetic metalloligand [Cr<sup>III</sup>L<sub>3</sub>] and the corresponding Ni<sup>II</sup> salt. The magnetic skeleton of each capsule describes a face-centred cube in which the eight Cr<sup>III</sup> and six Ni<sup>II</sup> ions occupy the eight vertices and six faces of the structure, respectively. Direct current magnetic susceptibility measurements on (**1**) reveal weak ferromagnetic interactions between the Cr<sup>III</sup> and Ni<sup>II</sup> ions, with  $J_{\text{Cr-Ni}} = +0.045 \text{ cm}^{-1}$ . EPR spectra are consistent with weak exchange, being dominated by the zero-field splitting of the Cr<sup>III</sup> ions. Excluding wheel-like structures, examples of large heterometallic clusters containing both Cr<sup>III</sup> and Ni<sup>II</sup> ions are rather rare, and we demonstrate that the use of metalloligands with predictable bonding modes allows for a modular approach to building families of related polymetallic complexes. Compounds (**1**)–(**3**) join the previously published, structurally related family of [M<sup>III</sup><sub>8</sub>M<sup>II</sup><sub>6</sub>] cubes, where M<sup>III</sup> = Cr, Fe and M<sup>II</sup> = Cu, Co, Mn, Pd.

**Keywords:** molecular magnetism; supramolecular chemistry; heterometallic clusters; magnetometry; EPR spectroscopy



**Citation:** O'Connor, H.M.; Sanz, S.; Scott, A.J.; Pitak, M.B.; Klooster, W.T.; Coles, S.J.; Chilton, N.F.; McInnes, E.J.L.; Lusby, P.J.; Weihe, H.; et al. [Cr<sup>III</sup><sub>8</sub>Ni<sup>II</sup><sub>6</sub>]<sup>n+</sup> Heterometallic Coordination Cubes. *Molecules* **2021**, *26*, 757. <https://doi.org/10.3390/molecules26030757>

Academic Editors: William T. A. Harrison, R. Alan Aitken and Paul Waddell

Received: 19 January 2021

Accepted: 30 January 2021

Published: 2 February 2021

**Publisher's Note:** MDPI stays neutral with regard to jurisdictional claims in published maps and institutional affiliations.

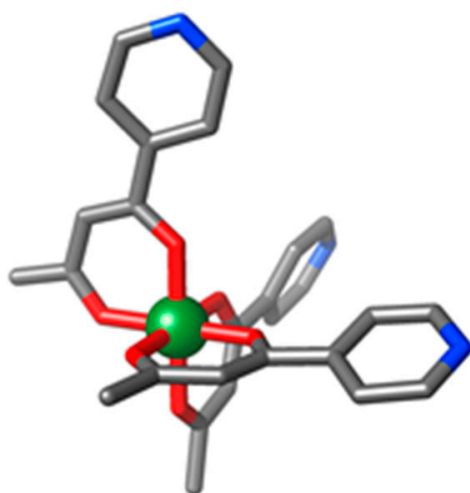


**Copyright:** © 2021 by the authors. Licensee MDPI, Basel, Switzerland. This article is an open access article distributed under the terms and conditions of the Creative Commons Attribution (CC BY) license (<https://creativecommons.org/licenses/by/4.0/>).

## 1. Introduction

Heterometallic coordination complexes have seen application in areas as diverse as metalloprotein chemistry [1,2], catalysis [3], porous materials [4,5], and magnetism [6]. The latter includes three-dimensional (3D) networks [7], two-dimensional (2D) sheets [8], one-dimensional (1D) chains [9], and zero-dimensional (0D) (molecular) polygons and polyhedra [10,11], investigating controllable exchange interactions [12], enhanced magnetocaloric effects [13], spin frustration [14], slow relaxation of the magnetisation [15,16], and quantum coherence timescales [17]. A search of the Cambridge Structural Database (CSD) reveals that heterometallic wheels of varying size and metal ratios dominate the chemistry of polymetallic clusters containing both Cr<sup>III</sup> and Ni<sup>II</sup> ions with a nuclearity of four or more. Examples include [Cr<sub>7</sub>Ni], [Cr<sub>9</sub>Ni], [Cr<sub>8</sub>Ni<sub>2</sub>], [Cr<sub>7</sub>Ni<sub>2</sub>], [Cr<sub>6</sub>Ni<sub>2</sub>], [Cr<sub>2</sub>Ni<sub>5</sub>], [CrNi<sub>6</sub>] wheels and discs (centred/Anderson wheels), and [Cr<sub>14</sub>Ni<sub>2</sub>] and [Cr<sub>28</sub>Ni<sub>4</sub>] 'linked rings' [18–23]. Surprisingly, the search reveals only two other unique structural motifs, a rather unusual [Cr<sub>3</sub>Ni<sub>2</sub>] linear complex [24], and an 'S-shaped' [Cr<sub>12</sub>Ni<sub>3</sub>] chain [25]. We have previously reported a metalloligand approach that enabled us to synthesise high-nuclearity heterometallic coordination capsules of paramagnetic transition metal ions in a

modular and predictable fashion [26–29]. This metalloligand, based on the tritopic  $[M^{III}L_3]$  moiety shown in Figure 1 (HL = 1-(4-pyridyl)butane-1,3-dione), features a tris(acac) coordinated octahedral transition metal ion, in which the ligand is functionalised with a *p*-pyridyl donor group. In the *fac*-isomer of this metalloligand, the three N-donor groups are orientated in such a way that combination with a square-planar metal ion leads to the entropically favoured self-assembly of a cubic structure [30]. Herein, we report the syntheses, structures, and magnetic properties of three novel tetradecanuclear  $[Cr^{III}_8Ni^{II}_6]^{n+}$  cubes, namely  $[Cr^{III}_8Ni^{II}_6L_{24}(H_2O)_{12}](NO_3)_{12}$  (**1**),  $[Cr^{III}_8Ni^{II}_6L_{24}(MeCN)_7(H_2O)_5](ClO_4)_{12}$  (**2**), and  $[Cr^{III}_8Ni^{II}_6L_{24}Cl_{12}]$  (**3**), which join the growing family of  $[M^{III}_8M^{II}_6]$  cubes constructed from  $[M^{III}L_3]$  and a variety of  $M^{II}$  salts ( $M^{III} = Cr, Fe$ ;  $M^{II} = Cu, Co, Mn, Pd$ ) [26–29].



**Figure 1.** Molecular structure of  $[M^{III}L_3]$ , where HL = 1-(4-pyridyl)butane-1,3-dione. Colour code:  $M^{III}$  = green, O = red, N = blue, C = grey. H-atoms have been omitted for clarity.

## 2. Materials and Methods

### 2.1. Synthesis

1-(4-pyridyl)butane-1,3-dione (HL) and the metalloligand  $[Cr^{III}L_3]$  were prepared by previously published procedures [26,31,32]. All reactions were carried out under aerobic conditions. Solvents and reagents were used as received from commercial suppliers. Caution: perchlorate salts of metal complexes with organic ligands are potentially explosive.

**Synthesis of  $[Cr^{III}_8Ni^{II}_6L_{24}(H_2O)_{12}](NO_3)_{12}$  (**1**).** To a solution of  $[Cr^{III}L_3]$  (54 mg, 0.1 mmol) in 10 mL of dichloromethane, a solution of  $Ni(NO_3)_2 \cdot 6H_2O$  (30 mg, 0.1 mmol) was added in 10 mL of methanol. The solution was stirred for 18 h before being filtered and allowed to stand. Dark orange X-ray quality crystals were obtained from the diffusion of diethyl ether into the mother liquor. Yield of (**1**) = 69%. Elemental analysis (%) calculated (found): C 46.16 (46.01) H 3.87 (3.78) N 8.97 (8.63).

**Synthesis of  $[Cr^{III}_8Ni^{II}_6L_{24}(MeCN)_7(H_2O)_5](ClO_4)_{12}$  (**2**).** To a solution of  $[Cr^{III}L_3]$  (108 mg, 0.2 mmol) in 10 mL of dichloromethane, a solution of  $Ni(ClO_4)_2 \cdot 6H_2O$  (73 mg, 0.2 mmol) was added in 10 mL of acetonitrile. The solution was stirred for 18 h before being filtered and allowed to stand. Brown X-ray quality crystals were obtained after 5 days from the diffusion of pentane into the mother liquor. Yield of (**2**) = 81%. Elemental analysis (%) calculated (found): C 44.34 (44.06) H 3.61 (3.59) N 6.97 (7.11).

**Synthesis of  $[Cr^{III}_8Ni^{II}_6L_{24}Cl_{12}]$  (**3**).** To a solution of  $[Cr^{III}L_3]$  (108 mg, 0.2 mmol) in 10 mL of dichloromethane, a solution of  $NiCl_2$  (20 mg, 0.15 mmol) was added in 10 mL of tetrahydrofuran. The solution was stirred for 18 h before being filtered and allowed to stand. Brown X-ray quality crystals were obtained after room temperature evaporation of the mother liquor for 5 days. Yield of (**3**) = 58%. Elemental analysis (%) calculated (found): C 51.01 (50.79) H 3.81 (3.71) N 6.61 (6.68).

## 2.2. Crystallographic Details

Single-crystal X-ray diffraction data were collected for (1)–(3) at  $T = 100$  K on a Rigaku AFC12 goniometer equipped with an enhanced sensitivity (HG) Saturn 724+ detector mounted at the window of an FR-E+ Superbright MoK $\alpha$  rotating anode generator with HF Varimax optics (70  $\mu\text{m}$  focus) [33]. The CrysAlisPro software package was used for instrument control, unit cell determination, and data reduction [34]. Due to very weak scattering power, single-crystal X-ray diffraction data for (1) and (2) were collected at  $T = 30.15$  K using a synchrotron source ( $\lambda = 0.6889$  Å) on the I19 beam line at Diamond Light Source on an undulator insertion device with a combination of double crystal monochromator, vertical and horizontal focussing mirrors, and a series of beam slits. The same software as above was used for data refinement. Crystals of all samples were sensitive to solvent loss, which resulted in crystal delamination and poor-quality X-ray diffraction data. To slow down crystal degradation, crystals of (1)–(3) were “cold-mounted” on MiTeGen Micromounts<sup>TM</sup> at  $T = 203$  K using Sigma-Aldrich Fomblin Y<sup>®</sup> LVAC (3300 mol. wt.), with the X-Temp 2 crystal cooling system attached to the microscope [35]. This procedure protected crystal quality and permitted collection of usable X-ray data. Unit cell parameters in all cases were refined against all data. Crystal structures were solved using Intrinsic Phasing as implemented in SHELXT [36]. All non-hydrogen atoms were refined with anisotropic displacement parameters, and all hydrogen atoms were added at calculated positions and refined using a riding model with isotropic displacement parameters based on the equivalent isotropic displacement parameter ( $U_{\text{eq}}$ ) of the parent atom. All three crystal structures contain large accessible voids and channels that are filled with diffuse electron density belonging to uncoordinated solvent, whose electron contribution was accounted for by the PLATON/SQUEEZE routine ((1) and (2)) [37], or by the SMTBX solvent masking routine, as implemented in OLEX2 software (3). To maintain reasonable molecular geometry, DFIX restraints were used in all three complexes.

Crystal Data for  $[\text{Cr}^{\text{III}}_8\text{Ni}^{\text{II}}_6\text{L}_{24}(\text{H}_2\text{O})_{12}](\text{NO}_3)_{12}$  (1).  $\text{C}_{216}\text{H}_{216}\text{Cr}_8\text{N}_{24}\text{Ni}_6\text{O}_{60}$ ,  $M_r = 4876.38$ , monoclinic,  $a = 25.754(3)$  Å,  $b = 41.336(5)$  Å,  $c = 43.217(5)$  Å,  $\alpha = 90^\circ$ ,  $\beta = 90.6450(10)^\circ$ ,  $\gamma = 90^\circ$ ,  $V = 46,004(9)$  Å<sup>3</sup>,  $Z = 4$ ,  $P2_1/n$ ,  $D_c = 0.704$  g cm<sup>-3</sup>,  $\mu = 9.18$  mm<sup>-1</sup>,  $T = 100.15(10)$  K, 370,995 reflections measured, 81,102 unique ( $R_{\text{int}} = 0.1902$ ), which were used in all calculations,  $wR_2$  (all data) = 0.3687, and  $R_1 [I > 2(I)] = 0.1242$ . CCDC 1977309.

Crystal Data for  $[\text{Cr}^{\text{III}}_8\text{Ni}^{\text{II}}_6\text{L}_{24}(\text{MeCN})_7(\text{H}_2\text{O})_5](\text{ClO}_4)_{12}$  (2).  $\text{C}_{230}\text{H}_{218}\text{Cr}_8\text{N}_{31}\text{Ni}_6\text{O}_{54}$ ,  $M_r = 5048.60$ , monoclinic,  $a = 25.788(6)$  Å,  $b = 41.606(9)$  Å,  $c = 45.869(11)$  Å,  $\alpha = 90^\circ$ ,  $\beta = 90.785(2)^\circ$ ,  $\gamma = 90^\circ$ ,  $V = 49,210(20)$  Å<sup>3</sup>,  $Z = 4$ ,  $P2_1/n$ ,  $D_c = 0.681$  g cm<sup>-3</sup>,  $\mu = 0.412$  mm<sup>-1</sup>,  $T = 100.15(10)$  K, 391,278 reflections measured, 85,150 unique ( $R_{\text{int}} = 0.2371$ ), which were used in all calculations,  $wR_2$  (all data) = 0.4444, and  $R_1 [I > 2(I)] = 0.1521$ . CCDC 1977311.

Crystal Data for  $[\text{Cr}^{\text{III}}_8\text{Ni}^{\text{II}}_6\text{L}_{24}\text{Cl}_{12}]$  (3).  $\text{C}_{216}\text{H}_{192}\text{Cl}_{12}\text{Cr}_8\text{N}_{24}\text{Ni}_6\text{O}_{48}$ ,  $M_r = 5085.58$ , triclinic,  $a = 28.171(16)$  Å,  $b = 30.225(16)$  Å,  $c = 32.40(2)$  Å,  $\alpha = 72.27(6)^\circ$ ,  $\beta = 72.08(6)^\circ$ ,  $\gamma = 64.04(6)^\circ$ ,  $V = 22,417(27)$  Å<sup>3</sup>,  $Z = 2$ ,  $P-1$ ,  $D_c = 0.753$  g cm<sup>-3</sup>,  $\mu = 0.543$  mm<sup>-1</sup>,  $T = 100.0(1)$  K, 134,344 reflections measured, 66,105 unique ( $R_{\text{int}} = 0.1446$ ), which were used in all calculations,  $wR_2$  (all data) = 0.5544, and  $R_1 [I > 2(I)] = 0.1938$ . CCDC 1977312.

## 2.3. Magnetic and Spectroscopic Measurements

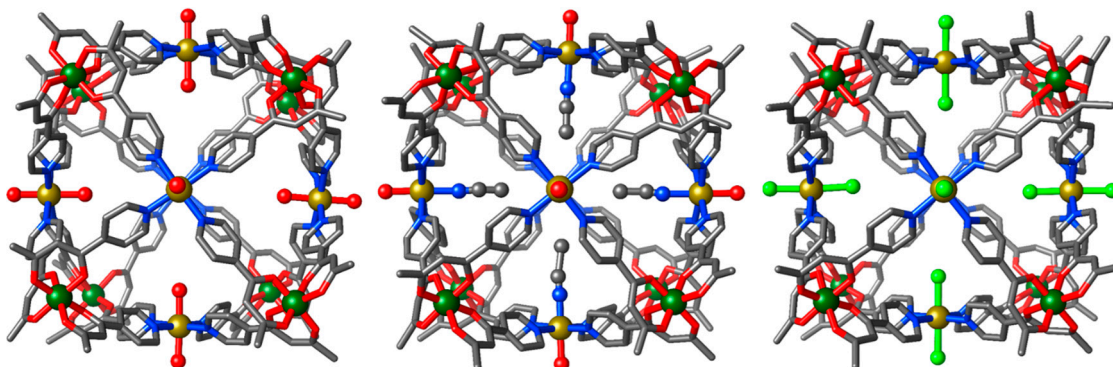
Direct current (dc) susceptibility and magnetisation data were measured on powdered, polycrystalline samples of (1) using a Quantum Design SQUID MPMS-XL magnetometer, operating between 1.8 and 300 K for dc applied magnetic fields ranging from 0 to 5 T. X-band EPR spectra were collected on powdered microcrystalline samples of (1) using a Bruker EMX spectrometer at the EPSRC UK National EPR Facility at The University of Manchester.

## 3. Results and Discussion

### 3.1. Structural Description

The heterometallic cubes  $[\text{Cr}^{\text{III}}_8\text{Ni}^{\text{II}}_6\text{L}_{24}(\text{H}_2\text{O})_{12}](\text{NO}_3)_{12}$  (1),  $[\text{Cr}^{\text{III}}_8\text{Ni}^{\text{II}}_6\text{L}_{24}(\text{MeCN})_7(\text{H}_2\text{O})_5](\text{ClO}_4)_{12}$  (2), and  $[\text{Cr}^{\text{III}}_8\text{Ni}^{\text{II}}_6\text{L}_{24}\text{Cl}_{12}]$  (3) were formed from the reaction of  $[\text{Cr}^{\text{III}}\text{L}_3]$

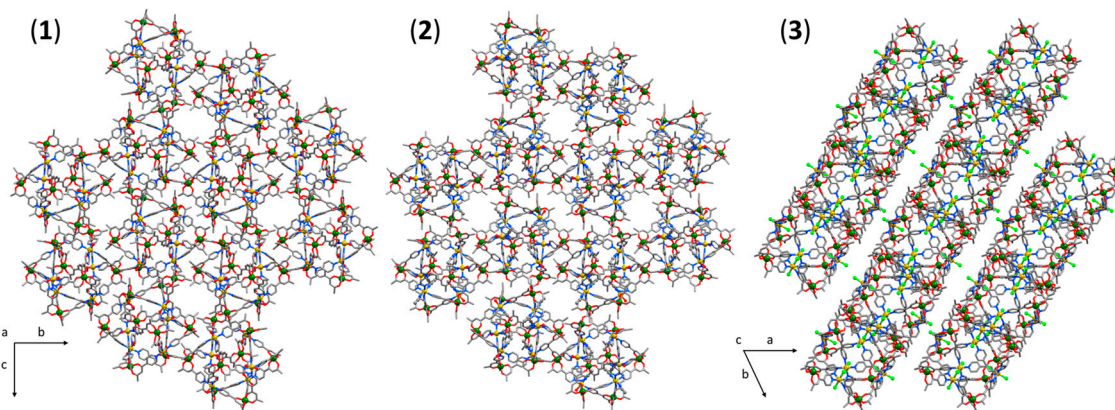
with the corresponding Ni<sup>II</sup> salt in CH<sub>2</sub>Cl<sub>2</sub>/MeOH, CH<sub>2</sub>Cl<sub>2</sub>/MeCN, and CH<sub>2</sub>Cl<sub>2</sub>/THF, respectively. All three structures (Figure 2) reveal a similar [Cr<sup>III</sup><sub>8</sub>Ni<sup>II</sup><sub>6</sub>] cube-like metallic skeleton, with the eight Cr<sup>III</sup> ions located at the corners and the six Ni<sup>II</sup> ions located on the faces, approximately 1.4–2.3 Å above the Cr···Cr···Cr···Cr plane. The internal cavity volume of the cube is approximately 1400 Å<sup>3</sup>.



**Figure 2.** From left to right, molecular structures of (1), (2), and (3). Colour code: Cr<sup>III</sup> = green, Ni<sup>II</sup> = yellow, O = red, N = blue, Cl = light green, C = grey. H-atoms have been omitted for clarity.

The Cr<sup>III</sup> ions are all octahedral, possessing {CrO<sub>6</sub>} coordination spheres with Cr<sup>III</sup>–O distances between 1.9 and 2.2 Å, and *cis/trans* angles in the range 82.7–97°/171.3–179.4°, respectively. The equatorial positions of the octahedral Ni<sup>II</sup> ions are occupied by four pyridyl donors from four distinct [Cr<sup>III</sup>L<sub>3</sub>] subunits, with Ni<sup>II</sup>–N distances in the range 1.9–3.0 Å. For (1) and (2), the axial positions are occupied by twelve water and twelve acetonitrile/water molecules (Ni<sup>II</sup>–O ≈ 2.1 Å; Ni<sup>II</sup>–N ≈ 2.1 Å), respectively. The cubes are therefore cationic (12+). The charge balancing nitrate or perchlorate anions for (1) and (2) respectively, are located both within the central cavity of the cube and in the void spaces between cubes. In contrast to (1) and (2), complex (3) is neutral, with the axial positions of the Ni<sup>II</sup> ions occupied by chloride anions (Ni<sup>II</sup>–Cl ≈ 2.7 Å).

There are several close intermolecular contacts (Figure 3) between the cages in the extended structures of (1)–(3). In (1), the closest inter-cluster contact is between the aromatic protons of the pyridyl group and the O-atom (2.3 Å) of a neighbouring L<sup>−</sup> ligand. In (2) and (3), the closest contact is between the protons of the metalloligand methyl group, and the O-atom of a neighbouring L<sup>−</sup> ligand (2.3 Å) and the protons of a neighbouring methyl group (2.3 Å), respectively. Several other close inter-cluster contacts between neighbouring cubes exist, for example: Ar–H···O ≈ 2.5 Å and C–H···O ≈ 2.7 Å for (1), H<sub>2</sub>C–H···O ≈ 2.5 Å and H<sub>2</sub>O···H–CH<sub>2</sub> ≈ 2.7 Å for (2), and Ar–H···Cl ≈ 2.7 Å and C–H···Cl ≈ 2.8 Å for (3).

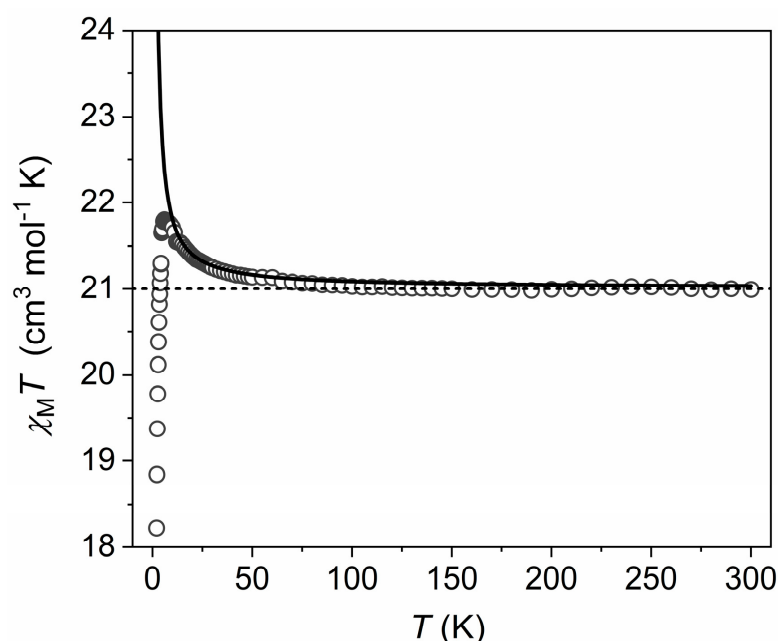


**Figure 3.** Packing diagrams of (1)–(3) viewed down the *a*-, *a*-, and *c*-axis, respectively. Colour code as in Figure 1.



### 3.2. Magnetic Properties

As complexes (1)–(3) are structurally analogous, and for the sake of brevity, we discuss only the behaviour of a representative example, complex (1). The dc molar magnetic susceptibility,  $\chi_M$ , of a polycrystalline sample of (1) was measured in an applied magnetic field,  $B$ , of 0.1 T, over the 2–300 K temperature,  $T$ , range. The experimental results are shown in Figure 4 in the form of the  $\chi_M T$  product versus temperature, where  $\chi_M = M/B$ , and  $M$  is the magnetization of the sample. Due to the loss of lattice solvent during the evacuation of the sample chamber of the SQUID magnetometer, leading to an uncertainty in the molar mass of the measured sample, the  $T = 300$  K  $\chi_M T$  product of (1) was scaled to  $21.00 \text{ cm}^3 \text{ mol}^{-1} \text{ K}$ , the expected value from the sum of Curie constants for a  $[\text{Cr}^{\text{III}}_8\text{Ni}^{\text{II}}_6]$  unit, with  $g_{\text{Cr}} = g_{\text{Ni}} = 2.0$ , where  $g_{\text{Cr}}$  and  $g_{\text{Ni}}$  are the  $g$ -factors of  $\text{Cr}^{\text{III}}$  and  $\text{Ni}^{\text{II}}$ , respectively. Note that this rescaled value has a maximum deviation of 15% from the unscaled data.



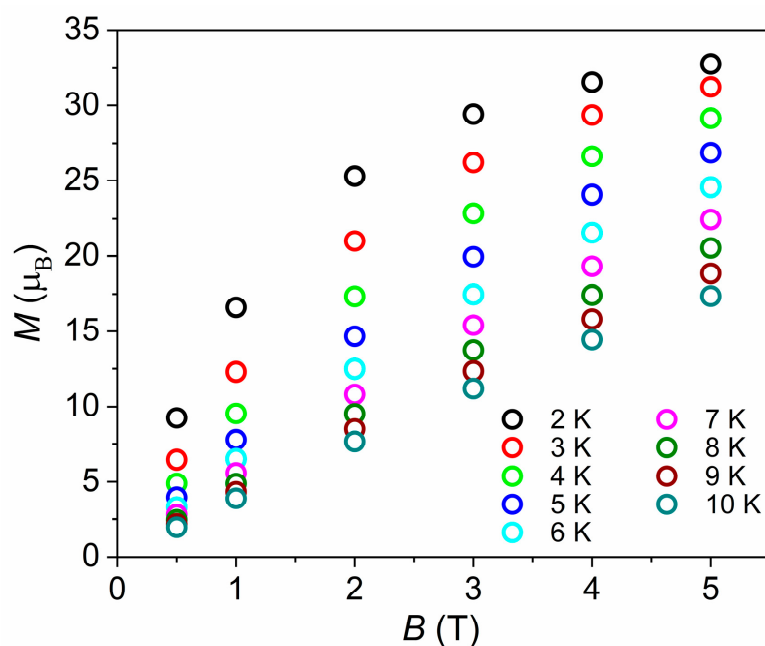
**Figure 4.** Plot of  $\chi_M T$  (open circles) versus  $T$  for complex (1), with the sum of the Curie constants of the uncorrelated ions and the best-fit data represented by the dashed and solid lines, respectively.

Upon cooling, the value of  $\chi_M T$  remains essentially constant to approximately  $T = 75$  K, where it begins to increase, reaching a maximum of  $21.8 \text{ cm}^3 \text{ mol}^{-1} \text{ K}$  at  $T = 6$  K. Below this temperature,  $\chi_M T$  falls rapidly to a minimum value of  $18.5 \text{ cm}^3 \text{ mol}^{-1} \text{ K}$  at  $T = 2.0$  K. The behaviour is suggestive of weak ferromagnetic exchange between the  $\text{Cr}^{\text{III}}$  and  $\text{Ni}^{\text{II}}$  ions, with the decrease in  $\chi_M T$  below 6 K attributed to intermolecular antiferromagnetic exchange interactions, and/or zero-field splitting (zfs) effects primarily associated with the  $\text{Ni}^{\text{II}}$  ions. Quantitative analysis of the susceptibility data via standard matrix diagonalization techniques is non-trivial due to the large nuclearity of the cluster and the associated enormous dimensions of the spin-Hamiltonian matrices. Even the total spin ( $S$ ) block matrices used in approaches based on Irreducible Tensor Operator algebra are of larger dimensions than what is realistic for exact numerical matrix diagonalization. Previously, we reported the use of computational techniques, known in theoretical nuclear physics as statistical spectroscopy [38], to analyse the structurally similar  $[\text{M}^{\text{III}}_8\text{M}^{\text{II}}_6]^{n+}$  ( $\text{M}^{\text{III}} = \text{Cr, Fe}$ ;  $\text{M}^{\text{II}} = \text{Co, Cu, Ni}$ ;  $n = 0\text{--}12$ ) cubes [26–28]. We now extend this methodology to quantify the exchange interactions present in (1). Due to the fact that the influence of the zfs of the  $\text{Ni}^{\text{II}}$  ions will mainly affect the measured properties at low temperatures, the use of the

isotropic spin-Hamiltonian (1) is sufficient to model the exchange interactions between  $\text{Cr}^{\text{III}}$  and  $\text{Ni}^{\text{II}}$  ions in the  $T = 300\text{--}6$  K region:

$$\hat{H}_{iso} = -2J_{\text{Cr-Ni}} \sum_{\text{allCr-Nipairs}} \hat{S}_{\text{Cr}} \cdot \hat{S}_{\text{Ni}} + \mu_{\text{B}} B g \sum_i \hat{S}_i^Z \quad (1)$$

with  $i$  running over all constitutive metal centres,  $g$  is the isotropic  $g$ -factor,  $\hat{S}$  is a spin-operator,  $J_{\text{Cr-M}}$  is the isotropic exchange parameter between  $\text{Cr}^{\text{III}}$  and  $\text{M}^{\text{II}}$  centres, and  $\mu_{\text{B}}$  is the Bohr magneton. We assume common  $g$ -factors for both  $\text{Cr}^{\text{III}}$  and  $\text{Ni}^{\text{II}}$  ( $g_{\text{Cr}} = g_{\text{Ni}} = 2.0$ ) since the 300 K  $\chi_{\text{M}}T$  product of (1) was scaled to the sum of its Curie constants, as explained above. We neglect any  $J_{\text{Cr-Cr}}$  and  $J_{\text{Ni-Ni}}$  terms as these centres are not connected as first neighbours. Using Hamiltonian (1),  $J_{\text{Cr-Ni}}$  was determined to be  $+0.045 \text{ cm}^{-1}$ . Variable-temperature and variable-field (VTVB) magnetization studies of (1) collected in the  $T = 2\text{--}10$  K and  $B = 0.5\text{--}5$  T temperature and field ranges (Figure 5) are consistent with this picture.  $M$  reaches a value of  $32.8 \mu_{\text{B}}$  at  $B = 5$  T and  $T = 2$  K, approaching the saturation value of  $36 \mu_{\text{B}}$ , consistent with relatively small exchange-induced splittings that lead to the  $m_S = 18$  projection of the  $S = 18$  total spin state, being the ground state at the highest measured magnetic field. The weak ferromagnetic exchange between the  $d^3 \text{Cr}^{\text{III}}$  ions and the  $d^8 \text{Ni}^{\text{II}}$  ions is as one would expect, mediated via the 1-(4-pyridyl)butane-1,3-dione ligand [26–28].

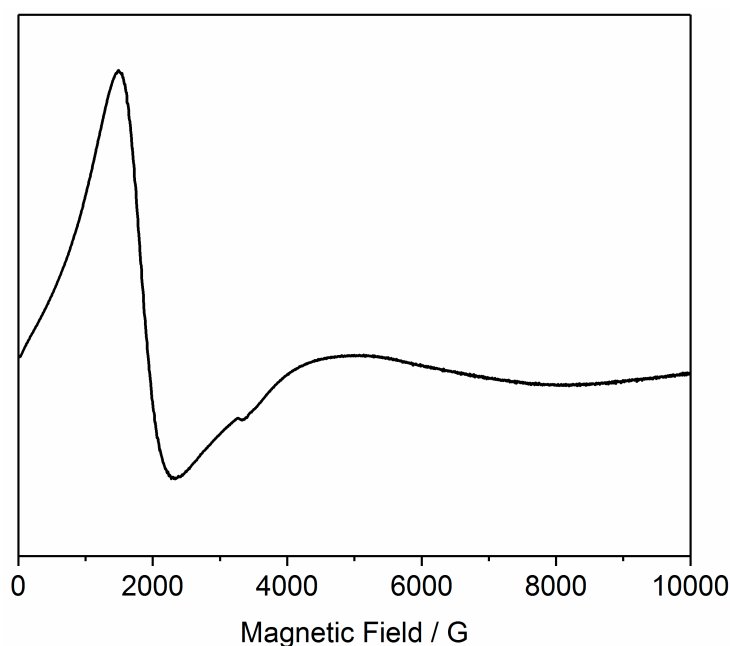


**Figure 5.** VTVB magnetisation data for (1) in the temperature and field ranges  $T = 2\text{--}10$  K and  $B = 0.5\text{--}5$  T.

### 3.3. EPR Spectroscopy

X-band EPR spectra of a powdered sample of (1) at 5 and 10 K are dominated by a feature at ca. 2 kG (Figure 6). This is similar to spectra from the isolated  $[\text{Cr}^{\text{III}}\text{L}_3]$  complex, and related  $[\text{Cr}^{\text{III}}_8\text{M}^{\text{II}}_6]$  and  $[\text{Cr}^{\text{III}}_2\text{M}^{\text{II}}_3]$  species [26,29], and arises from the  $\text{Cr}^{\text{III}}$  ( $S = 3/2$ ) ions with a near-axial zero-field splitting of  $|D_{\text{Cr}}|$  ca.  $0.5\text{--}0.6 \text{ cm}^{-1}$ . This is only consistent with a weak exchange interaction  $|J_{\text{Cr-Ni}}|$  with respect to  $|D_{\text{Cr}}|$ , and hence consistent with the magnetic data. There are no clear features arising from the  $\text{Ni}^{\text{II}}$  ( $S = 1$ ) ions, which implies that  $|D_{\text{Ni}}|$  must be much larger than the microwave energy. We also observed this for a related  $[\text{Fe}^{\text{III}}_8\text{M}^{\text{II}}_6]$  cube, which only showed EPR features due to  $\text{Fe}^{\text{III}}$  [28]. This is consistent with  $|D_{\text{Ni}}|$  values of  $5\text{--}10 \text{ cm}^{-1}$  determined from magnetization studies

of isolated  $[\text{Ni}^{\text{II}}(\text{pyridine})_4\text{X}_2]$  complexes [39], and with high-field EPR studies of  $\text{Ni}^{\text{II}}$  complexes with mixed N,O-donor sets [40].



**Figure 6.** X-band (*ca.* 9.4 GHz) EPR spectrum of a powdered sample of (1) at 5 K.

#### 4. Conclusions

We have shown that the modular self-assembly of  $[\text{M}^{\text{III}}\text{L}_3]$  metalloligands with simple  $\text{M}^{\text{II}}$  salts can be exploited to construct large heterometallic coordination compounds of  $\text{Cr}^{\text{III}}$  and  $\text{Ni}^{\text{II}}$ . Compounds (1)–(3) join a growing family of  $[\text{M}^{\text{III}}_8\text{M}^{\text{II}}_6]$  cubes, where  $\text{M}^{\text{III}} = \text{Cr}$  and  $\text{Fe}$  and  $\text{M}^{\text{II}} = \text{Cu}, \text{Co}, \text{Mn}, \text{Pd},$  and  $\text{Ni}$ . The ability to build families of isostructural complexes containing different combinations of paramagnetic (and diamagnetic) metal centres aids the qualitative and quantitative understanding of magnetic properties and the underlying structural parameters that govern behaviour. Examples of large, heterometallic cages in which the  $3d$  metal ions can be exchanged with other  $3d$  metal ions are extremely rare.

Magnetic susceptibility and magnetization data show the presence of weak ferromagnetic exchange between the  $\text{Cr}^{\text{III}}$  and  $\text{Ni}^{\text{II}}$  ions, with  $J_{\text{Cr-Ni}} = +0.045 \text{ cm}^{-1}$ . EPR spectroscopy is consistent with the exchange interactions being much weaker than the zero-field splittings of both the  $\text{Cr}^{\text{III}}$  and  $\text{Ni}^{\text{II}}$  ions.

**Author Contributions:** E.K.B., P.J.L., H.M.O. and S.S. designed the study. H.M.O., S.S. and A.J.S. performed the synthetic work. M.B.P., W.T.K. and S.J.C. performed the crystallographic work. H.W. and S.P. performed the magnetometry measurements and associated analysis. N.F.C. and E.J.L.M. performed the EPR spectroscopic experiments and associated analysis. H.M.O. and E.K.B. wrote the paper with input from all authors. All authors have read and agreed to the published version of the manuscript.

**Funding:** This research was funded by the EPSRC (UK), grant numbers EP/N01331X/1 and EP/P025986/1, and by the VILLUM FONDEN (Denmark), grant 13376. We also thank the EPSRC for funding the UK National EPR Facility.

**Institutional Review Board Statement:** Not applicable.

**Informed Consent Statement:** Not applicable.

**Data Availability Statement:** The data presented in this study are available on request from the corresponding authors.

**Conflicts of Interest:** The authors declare that there is no conflict of interest.

## References

1. Barton, B.E.; Whaley, C.M.; Rauchfuss, T.B.; Gray, D.L. Nickel–Iron Dithiolato Hydrides Relevant to the [NiFe]-Hydrogenase Active Site. *J. Am. Chem. Soc.* **2009**, *131*, 6942–6943. [[CrossRef](#)]
2. Canaguier, S.; Field, M.; Oudart, Y.; Pécaut, J.; Fontecave, M.; Artero, V. A structural and functional mimic of the active site of NiFe hydrogenases. *Chem. Commun.* **2010**, *46*, 5876–5878. [[CrossRef](#)]
3. Buchwalter, P.; Rosé, J.; Braunstein, P. Multimetallic Catalysis Based on Heterometallic Complexes and Clusters. *Chem. Rev.* **2015**, *115*, 28–126. [[CrossRef](#)]
4. Rice, A.M.; Leith, G.A.; Ejegbavwo, O.A.; Dolgoplova, E.A.; Shustova, N.B. Heterometallic Metal–Organic Frameworks (MOFs): The Advent of Improving the Energy Landscape. *ACS Energy Lett.* **2019**, *4*, 1938–1946. [[CrossRef](#)]
5. Zhang, Y.Y.; Gao, W.X.; Lin, L.; Jin, G.X. Recent advances in the construction and applications of heterometallic macrocycles and cages. *Coord. Chem. Rev.* **2017**, *344*, 323–344. [[CrossRef](#)]
6. Vigato, P.A.; Tamburini, S. Advances in acyclic compartmental ligands and related complexes. *Coord. Chem. Rev.* **2008**, *252*, 1871–1995. [[CrossRef](#)]
7. Ferlay, S.; Mallah, T.; Ouahès, R.; Veillet, P.; Verdaguer, M. A room-temperature organometallic magnet based on Prussian blue. *Nature* **1995**, *378*, 701–703. [[CrossRef](#)]
8. Alexandru, M.-G.; Visinescu, D.; Shova, S.; Lloret, F.; Julve, M.; Andruh, M. Two-Dimensional Coordination Polymers Constructed by [Ni<sup>II</sup>Ln<sup>III</sup>] Nodes and [W<sup>IV</sup>(bpy)(CN)<sub>6</sub>]<sup>2-</sup> Spacers: A Network of [Ni<sup>II</sup>Dy<sup>III</sup>] Single Molecule Magnets. *Inorg. Chem.* **2013**, *52*, 11627–11637. [[CrossRef](#)]
9. Yao, M.-X.; Wei, Z.-Y.; Gu, Z.-G.; Zheng, Q.; Xu, Y.; Zuo, J.-L. Syntheses, Structures, and Magnetic Properties of Low-Dimensional Heterometallic Complexes Based on the Versatile Building Block [(Tp)Cr(CN)<sub>3</sub>]<sup>-</sup>. *Inorg. Chem.* **2011**, *50*, 8636–8644. [[CrossRef](#)]
10. Liu, W.; Wang, C.; Li, Y.; Zuo, J.; You, X. Structural and Magnetic Studies on Cyano-Bridged Rectangular Fe<sub>2</sub>M<sub>2</sub> (M = Cu, Ni) Clusters. *Inorg. Chem.* **2006**, *45*, 10058–10065. [[CrossRef](#)]
11. Beltran, L.M.C.; Long, J.R. Directed Assembly of Metal–Cyanide Cluster Magnets. *Acc. Chem. Res.* **2005**, *38*, 325–334. [[CrossRef](#)] [[PubMed](#)]
12. Rebilly, J.N.; Mallah, T. Synthesis of Single-Molecule Magnets Using Metalocyanates. *Single-Mol. Magn. Relat. Phenom.* **2006**, 103–131. [[CrossRef](#)]
13. Evangelisti, M.; Brechin, E.K. Recipes for enhanced molecular cooling. *Dalton Trans.* **2010**, *39*, 4672–4676. [[CrossRef](#)] [[PubMed](#)]
14. Schnack, J. Effects of frustration on magnetic molecules: A survey from Olivier Kahn until today. *Dalton Trans.* **2010**, *39*, 4677–4686. [[CrossRef](#)] [[PubMed](#)]
15. Milios, C.J.; Winpenny, R.E.P. Cluster-Based Single-Molecule Magnets. *Mol. Nanomagnets Relat. Phenom.* **2015**, 1–109. [[CrossRef](#)]
16. Coulon, C.; Pianet, V.; Urdampilleta, M.; Clérac, R. Single-Chain Magnets and Related Systems. *Mol. Nanomagnets Relat. Phenom.* **2015**, 143–184. [[CrossRef](#)]
17. Gaita-Ariño, A.; Luis, F.; Hill, S.; Coronado, E. Molecular spins for quantum computation. *Nat. Chem.* **2019**, *11*, 301–309. [[CrossRef](#)]
18. Larsen, F.K.; McInnes, E.J.L.; Mkami, H.E.; Overgaard, J.; Piligkos, S.; Rajaraman, G.; Rentschler, E.; Smith, A.A.; Boote, V.; Jennings, M.; et al. Synthesis and Characterization of Heterometallic {Cr<sub>7</sub>M} Wheels. *Angew. Chem. Int. Ed.* **2003**, *115*, 105–109. [[CrossRef](#)]
19. Garlatti, E.; Guidi, T.; Ansbro, S.; Santini, P.; Amoretti, G.; Ollivier, J.; Mutka, H.; Timco, G.; Vitorica-Yrezabal, I.J.; Whitehead, G.F.S.; et al. Portraying entanglement between molecular qubits with four-dimensional inelastic neutron scattering. *Nat. Commun.* **2017**, *8*, 14543. [[CrossRef](#)]
20. Timco, G.A.; McInnes, E.J.L.; Pritchard, R.G.; Tuna, F.; Winpenny, R.E.P. Heterometallic Rings Made From Chromium Stick Together Easily. *Angew. Chem. Int. Ed.* **2008**, *47*, 9681–9684. [[CrossRef](#)]
21. Timco, G.A.; Batsanov, A.S.; Larsen, F.K.; Murn, C.A.; Overgaard, J.; Teat, S.J.; Winpenny, R.E.P. Influencing the nuclearity and constitution of heterometallic rings via templates. *Chem. Commun.* **2005**, 3649–3651. [[CrossRef](#)] [[PubMed](#)]
22. Fraser, H.W.L.; Nichol, G.S.; Uhrin, D.; Nielsen, U.G.; Evangelisti, M.; Schnack, J.; Brechin, E. Order in disorder: Solution and solid-state studies of [M<sup>III</sup><sub>2</sub>M<sup>II</sup><sub>5</sub>] wheels (M<sup>III</sup> = Cr, Al; M<sup>II</sup> = Ni, Zn). *Dalton Trans.* **2018**, *47*, 11834–11842. [[CrossRef](#)] [[PubMed](#)]
23. Kakaroni, F.E.; Collet, A.; Sakellari, E.; Tzimopoulos, D.I.; Siczek, M.; Lis, T.; Murri, M.; Milios, C.J. Constructing Cr<sup>III</sup>-centered heterometallic complexes: [Ni<sup>II</sup><sub>6</sub>Cr<sup>III</sup>] and [Co<sup>II</sup><sub>6</sub>Cr<sup>III</sup>] wheels. *Dalton Trans.* **2018**, *47*, 58–61. [[CrossRef](#)] [[PubMed](#)]
24. Manole, O.S.; Batsanov, A.S.; Struchkov, Y.T.; Timko, G.A.; Synzheryan, L.D.; Gerbelev, N.V. Synthesis and crystalline-structure of pentanuclear heterometallic pivaltoacetylacetonate complexes. *Koord. Khim.* **1994**, *20*, 231–237.
25. Heath, S.L.; Laye, R.H.; Murn, C.A.; Lima, N.; Sessoli, R.; Shaw, R.; Teat, S.J.; Timco, G.A.; Winpenny, R.E.P. Templating Open- and Closed-Chain Structures around Metal Complexes of Macrocycles. *Angew. Chem. Int. Ed.* **2004**, *43*, 6132–6135. [[CrossRef](#)]
26. Sanz, S.; O'Connor, H.M.; Pineda, E.M.; Pedersen, K.S.; Nichol, G.S.; Mønsted, O.; Weihe, H.; Piligkos, S.; McInnes, E.J.L.; Lusby, P.J.; et al. [Cr<sup>III</sup><sub>8</sub>M<sup>II</sup><sub>6</sub>]<sup>12+</sup> Coordination Cubes (M<sup>II</sup> = Cu, Co). *Angew. Chem. Int. Ed.* **2015**, *54*, 6761–6764. [[CrossRef](#)]
27. Sanz, S.; O'Connor, H.M.; Comar, P.; Baldansuren, F.T.A.; Pitak, M.B.; Coles, S.J.; Weihe, H.; Chilton, N.F.; McInnes, E.J.L.; Lusby, P.J.; et al. Modular [Fe<sup>III</sup><sub>8</sub>M<sup>II</sup><sub>6</sub>]<sup>n+</sup> (M<sup>II</sup> = Pd, Co, Ni, Cu) Coordination Cages. *Inorg. Chem.* **2018**, *57*, 3500–3506. [[CrossRef](#)]
28. O'Connor, H.M.; Sanz, S.; Pitak, M.B.; Coles, S.J.; Nichol, G.S.; Piligkos, S.; Lusby, P.J.; Brechin, E.K. [Cr<sup>III</sup><sub>8</sub>M<sup>II</sup><sub>6</sub>]<sup>n+</sup> (M<sup>II</sup> = Cu, Co) face-centred, metallosupramolecular cubes. *CrystrEngComm* **2016**, *18*, 4914–4920. [[CrossRef](#)]



29. Sanz, S.; O'Connor, H.M.; Martí-Centelles, V.; Comar, P.; Pitak, M.B.; Coles, S.J.; Lorusso, G.; Palacios, E.; Evangelisti, M.; Baldansuren, F.T.A.; et al.  $[M^{III}_2M^{II}_3]^{n+}$  trigonal bipyramidal cages based on diamagnetic and paramagnetic metalloligands. *Chem. Sci.* **2017**, *8*, 5526–5535. [[CrossRef](#)]
30. Chakrabarty, R.; Mukherjee, P.S.; Stang, P.J. Supramolecular Coordination: Self-Assembly of Finite Two- and Three-Dimensional Ensembles. *Chem. Rev.* **2011**, *111*, 6810–6918. [[CrossRef](#)]
31. Wu, H.-B.; Wang, Q.-M. Construction of Heterometallic Cages with Tripodal Metalloligands. *Angew. Chem. Int. Ed.* **2009**, *48*, 7343–7345. [[CrossRef](#)] [[PubMed](#)]
32. Singh, B.; Leshner, G.Y.; Pluncket, K.C.; Pagani, E.D.; Bode, D.C.; Bentley, R.G.; Connell, M.J.; Hamel, L.T.; Silver, P.J. Novel cAMP PDE III inhibitors: 1,6-naphthyridin-2(1H)-ones. *J. Med. Chem.* **1992**, *35*, 4858–4865. [[CrossRef](#)] [[PubMed](#)]
33. Coles, S.J.; Gale, P.A. Changing and challenging times for service crystallography. *Chem. Sci.* **2011**, *3*, 683–689. [[CrossRef](#)]
34. Rigaku, O.; CrysAlis, P.R.O.; Rigaku Oxford Diffraction. CrysAlisPro. 2016. Available online: <https://www.rigaku.com/zh-hans/products/smc/crysalis> (accessed on 18 January 2021).
35. Kottke, T.; Stalke, D. Crystal handling at low temperatures. *J. Appl. Crystallogr.* **1993**, *26*, 615–619. [[CrossRef](#)]
36. Sheldrick, G.M. SHELXT—Integrated space-group and crystal-structure determination. *Acta Cryst.* **2015**, *71*, 3–8. [[CrossRef](#)]
37. Dolomanov, O.V.; Blake, A.J.; Champness, N.R.; Schröder, M. OLEX: New software for visualization and analysis of extended crystal structures. *J. Appl. Crystallogr.* **2003**, *36*, 1283–1284. [[CrossRef](#)]
38. Wong, S.S.M. *Nuclear Statistical Spectroscopy*; Oxford University Press: Oxford, UK; Clarendon Press: Oxford, UK, 1986.
39. Otieno, T.; Thompson, R.C. Antiferromagnetism and metamagnetism in 1,4-diazine and pyridine complexes of nickel(II). *Can. J. Chem.* **1995**, *73*, 275–283. [[CrossRef](#)]
40. Krzystek, J.; Ozarowski, A.; Telser, J. Multi-frequency, high-field EPR as a powerful tool to accurately determine zero-field splitting in high-spin transition metal coordination complexes. *Coord. Chem. Rev.* **2006**, *250*, 2308–2324. [[CrossRef](#)]